

Suter, Naiana ; Stebel, Sophie ; Rianna, Carmela ; Radmacher, Manfred ; Brüggemann, Dorothea

Spatial patterning of nanofibrous collagen scaffolds modulates fibroblast morphology

Journal Article as: peer-reviewed accepted version (Postprint)

DOI of this document* (secondary publication): <https://doi.org/10.26092/elib/3647>

Publication date of this document: 07/02/2025

* for better findability or for reliable citation

Recommended Citation (primary publication/Version of Record) incl. DOI:

Naiana Suter, Sophie Stebel, Carmela Rianna, Manfred Radmacher and Dorothea Brüggemann.
Spatial patterning of nanofibrous collagen scaffolds modulates fibroblast morphology,
Biofabrication, Volume 13, 2020, 015007, ISSN 1758-5090, <https://doi.org/10.1088/1758-5090/abb744>

Please note that the version of this document may differ from the final published version (Version of Record/primary publication) in terms of copy-editing, pagination, publication date and DOI. Please cite the version that you actually used. Before citing, you are also advised to check the publisher's website for any subsequent corrections or retractions (see also <https://retractionwatch.com/>).

This is the Accepted Manuscript version of an article accepted for publication in Biofabrication. IOP Publishing Ltd is not responsible for any errors or omissions in this version of the manuscript or any version derived from it. The Version of Record is available online at <https://doi.org/10.1088/1758-5090/abb744>.

This document is made available under a Creative Commons licence.

The license information is available online: <https://creativecommons.org/licenses/by-nc-nd/4.0/>

Take down policy

If you believe that this document or any material on this site infringes copyright, please contact publizieren@suub.uni-bremen.de with full details and we will remove access to the material.

PAPER

Spatial patterning of nanofibrous collagen scaffolds modulates fibroblast morphology

Naiana Suter¹, Sophie Stebel², Carmela Rianna¹, Manfred Radmacher¹ and Dorothea Brüggemann^{1,3} 

¹ Institute for Biophysics, University of Bremen, Otto-Hahn-Allee 1, Bremen 28359, Germany

² University of Applied Sciences Bonn-Rhein-Sieg, Department of Natural Sciences, Grantham-Allee 20, Sankt Augustin 53757, Germany

³ MAPEX Center for Materials and Processes, University of Bremen, Bremen 28359, Germany

E-mail: brueggemann@uni-bremen.de

Keywords: self-assembly, 3D cell culture, tissue engineering, protein pattern, nanotopography, extracellular matrix

Supplementary material for this article is available [online](#)

Abstract

Current knowledge about cell-biomaterial interactions is often based on two-dimensional (2D) cell culture systems like protein-coated glass slides. However, such smooth surfaces cannot mimic the nanofibrous environment of the native extracellular matrix (ECM). It is therefore a major challenge to transfer the results from 2D surfaces to 3D protein scaffolds with biomimetic nanofiber architecture. To understand the influence of different protein topographies on the cell response we introduce a new process to fabricate binary collagen scaffolds of variable thickness with spatially controlled regions of nanofibrous and smooth topography. We used pH-induced self-assembly to prepare collagen nanofibers with diameters between 130 and 150 nm on glass surfaces, which were partly covered with a polymer mask. After cross-linking with glutaraldehyde, smooth collagen films were prepared on the remaining glass regions. Atomic force microscopy revealed a much lower surface roughness of smooth collagen compared to nanofibers. Subsequently, we studied the viability, morphology and migration of 3T3 fibroblasts on both collagen topographies. We found small, elongated fibroblasts with few, long filopodia on collagen nanofibers whereas large, flat fibroblasts with many short filopodia were observed on smooth collagen. Actin stress fibers on collagen nanofibers were substantially reduced in comparison to smooth collagen. Live cell tracking revealed that fibroblasts on thin nanofibrous collagen migrated faster than on smooth collagen. In summary, binary collagen scaffolds enabled us for the first time to study cell responses to topographical cues on a single protein scaffold. In future, it will be intriguing to transfer our patterning process to other proteins to study fundamental principles of topography-dependent cell recognition processes.

1. Introduction

Controlling the interaction of cells with biomaterials is one of the key challenges in regenerative medicine to promote tissue repair [1]. Besides biochemical and mechanical cues, cell behavior is modulated by the scaffold topography on different length scales [1–3]. Cell adhesion, for instance, is steered by topographic stimuli in the nano- and micrometer range [2]. During adhesion, filopodia play a pivotal role in cell signaling [3], recognition of topographical features [4] and in focal adhesion formation [5, 6]. Nanotopographies also have a major effect on stem cell adhesion and differentiation [7, 8]. Microtopographies,

on the other hand, are known to affect whole cell morphology [2] and can induce reprogramming of neuronal cells [9] or influence macrophage polarization, thus modulating the immune response to biomaterials [10].

New facets in the control of cell functions with two-dimensional (2D)-structured biomaterials have evolved from nano- and microstructuring techniques like electron beam lithography, microcontact printing or nanoimprint lithography, often using synthetic substrate materials [11, 12]. Such 2D topographies were also coated with different proteins to promote integrin-mediated cell adhesion and migration [13]. Nevertheless, in native tissues, cells are surrounded

by the extracellular matrix (ECM), a dense and porous three-dimensional (3D) network of protein nanofibers and polysaccharides [14–16]. In various tissues like bone, tendon or the dermis, collagen nanofibers assemble into ordered fiber bundles, which exhibit diameters of several micrometers [17, 18]. Despite the native 3D environment, current knowledge on cellular interactions with biomaterials, in particular, on contact guidance and filopodia dynamics, has mainly been obtained by experiments in 2D cell culture systems with rigid substrates like glass [19–21]. However, changes in filopodia formation in dependence of a 2D or 3D environment of varying topography can significantly alter cell adhesion, signaling and migration [22, 23]. As a consequence, it is still not understood in detail how filopodia recognize topographical features in their native matrix environment to direct cell growth [4, 19]. Moreover, it needs to be elucidated how closely mechanical and topographical signals of the ECM are intertwined when they steer cell behavior [24]. Therefore, the design of future biomaterials requires the development of new tools and substrate designs to understand how filopodia probe complex 3D environments and how cell growth is regulated in 3D matrices across different length scales [19, 21, 25, 26].

As the most abundant protein in the ECM, collagen is a well-established coating in conventional 2D cell culture systems [15]. So far, collagen films were also used to coat micropatterns on substrate materials like glass, agarose, polydimethylsiloxane (PDMS) or self-assembled monolayers (SAMs) [27–30]. Moreover, collagen can be assembled into porous networks of nanofibers by raising pH and ionic strength in an acidic solution [31, 32]. Depending on the pH conditions, such collagen nanofibers exhibit typical diameters between 80 and 200 nm [33], which resemble the native ECM architecture [34]. With these features, nanofibrous collagen networks have evolved into an important model system for a physiologically relevant microenvironment with tissue-like mechanical and structural features [25, 26, 35]. Therefore, collagen nanofibers have already been used in cell culture studies with fibroblasts and endothelial cells, often using smooth collagen as reference substrates [36–39]. Nevertheless, this experimental setup did not allow to analyze time-dependent cell reactions to topographical changes on the same substrate.

Hence, to enable tissue engineers to directly transfer cell culture results from smooth protein substrates into fibrous matrices, new scaffold designs are required, which combine smooth and nanofibrous topographies in a single protein scaffold. Building up on the established findings of fibroblast interaction with nanofibrous collagen matrices [36–38] we have introduced a new process to fabricate collagen scaffolds with spatially controlled regions of smooth and nanofibrous surface topography. Using this new

topographical 2D scaffold platform, we studied the interaction with NIH 3T3 fibroblasts and observed a direct influence of the underlying topography on the cell morphology and filopodia outgrowth.

2. Materials and methods

2.1. Preparation of collagen scaffolds

Glass coverslips with a diameter of 15 mm (VWR, Darmstadt, Germany) were cleaned with H_2SO_5 (piranha solution), which was freshly prepared by mixing 95% sulfuric acid with 30% hydrogen peroxide solution (both VWR) in a 3:1 ratio. Cleaned glass coverslips were stored in deionized water from a TKA water purification system (Thermo Fisher Scientific, Schwerte, Germany) and dried with nitrogen directly before further use. Collagen stock solutions with 5 mg ml^{-1} and 1 mg ml^{-1} were prepared by dissolving collagen type 1 from calf skin (Sigma Aldrich, Munich, Germany) in 5% acetic acid solution (Carl Roth GmbH, Karlsruhe, Germany). Collagen nanofibers were prepared by the established method of self-assembly [31, 32]. First, $100 \mu\text{l}$ of 10x phosphate buffered saline solution (PBS) at pH 7.4 (PBS, Life Technologies Europe BV, Netherlands) was added to the glass, followed by $100 \mu\text{l}$ collagen solution in acetic acid. During self-assembly, samples were placed in an ultrasonic bath (Branson Ultrasonics, Danbury, USA) for 20 min to increase the surface coverage. Collagen films with smooth topography were prepared by incubating $100 \mu\text{l}$ 0.5% acetic acid solution with $100 \mu\text{l}$ collagen solution on a piranha-cleaned coverslip. All collagen samples were dried overnight under ambient conditions and were cross-linked for 30 min using 2% (v/v) glutaraldehyde (GA) (AppliChem GmbH, Germany) in 10x PBS. Aldehyde residues were removed by three washing steps with 200 mM NH_4HCO_3 (Carl Roth GmbH) for 10 min each. Prior to further analysis, collagen scaffolds were dried under ambient conditions.

To prepare binary collagen scaffolds with smooth and nanofibrous topography, one half of a glass slide was covered with a polymer mask of Fixogum (Marabu GmbH + Co. KG, Germany). Collagen nanofibers were assembled with PBS on the accessible glass surface under the influence of ultrasonication and were dried overnight. Subsequently, fibers were cross-linked, washed, and the mask was removed. To prepare a smooth collagen film on the other half of the substrate the remaining glass surface was coated with collagen in acetic acid and dried overnight. Another fixation and washing step were carried out until the binary scaffolds were finally dried overnight.

2.2. Atomic force microscopy

An MFP-3D atomic force microscope (AFM, Asylum Research, Santa Barbara, CA, USA) was used to analyze the topography of collagen scaffolds in dry and wet conditions. An optical light microscope was

combined with the AFM to control the scanning process. The surface topography of dried collagen was analyzed in ambient air. Topographical analysis in a wet environment was carried out after rehydration in DMEM cell culture medium (Biochrom GmbH, Germany). For AFM scanning, silicon nitride cantilevers (MLCT Bio, Bruker, Wissembourg, France) with a nominal resonant frequency of 38 kHz (in air) and a nominal spring constant of 0.1 N m^{-1} were used. Height profiles were measured in contact mode with a scan rate of 1 line per second at 256 lines per frame (frame size $5 \mu\text{m}^2$) and were subsequently averaged over a ROI of $1 \mu\text{m}^2$.

2.3. Cell culture

Adherent NIH 3T3 mouse fibroblasts (ATCC CRL1658, a kind gift from Louis Lim, Institute of Molecular and Cell Biology ASTAR Singapore) were used as model system to study the interaction with topographically patterned collagen scaffolds. Prior to cell seeding, collagen scaffolds and bare glass coverslips to be used as controls were sterilized in the UV light of a laminar flow cabinet (ESI Flufrance) for 30 min. Fibroblasts were cultivated using DMEM cell culture medium (Biochrom GmbH, Germany) with additional 1% (v/v) penicillin and streptomycin and 10% (v/v) fetal bovine serum (FBS) (Sigma-Aldrich Chemie GmbH, Germany). The cells were subcultured at a confluence of approximately 80% and transferred into a fresh 25 cm^2 cell culture flask (Sarstedt, Nümbrecht, Germany) for further cultivation under physiological conditions. For splitting, cell medium was aspirated, and the cell layer was washed carefully with PBS followed by incubation with 1 ml trypsin/EDTA solution (1% (v/v), diluted in PBS) for 3 min at 37°C . The enzymatic reaction was stopped through dilution with DMEM medium, followed by centrifugation at 1300 rpm for 3 min. For further cultivation approximately 1.2×10^5 cells were seeded in cell culture flasks with 25 cm^2 . For live/dead staining and morphology studies, fibroblasts were seeded onto collagen scaffolds and glass references in 12-well-plates (Greiner-Bio-One, Germany) at a density of 7500 cells per cm^2 and incubated for 24 h, 48 h and 72 h, respectively, at 37°C with 5% CO_2 . Live/dead staining and cell size analysis were performed only on thin substrates prepared with 0.5 mg ml^{-1} collagen to reduce the intrinsic autofluorescence of collagen type I [40] cross-linked with GA [41], while all other experiments were conducted with thin and thick collagen scaffolds. For AFM analysis of cell mechanics and cell migration tracking, a density of 12 500 cells per cm^2 was used. Cell mechanics were measured between 24 h and 33 h incubation time. Cell migration analysis was carried out between 24 h and 44 h.

2.4. Fibroblast morphology

Cell nuclei and actin filaments were fluorescently stained to analyze the cell morphology. Cells were

fixed in 2% (v/v) GA in PBS for 30 min and washed with PBS. Then, actin was stained with phalloidin (ActinGreen™ ReadyProbes® Reagent, Life Technologies Europe BV, Netherlands) for 30 min, followed by nuclei staining with DAPI (NucBlue® Live ReadyProbes™ Reagent, Life Technologies) for 30 min. After washing in PBS, the stained samples were mounted onto glass slides with Prolong™ Gold antifade mounting medium (Fisher Scientific GmbH, Germany). Subsequently, fibroblasts were imaged at 40x and 60x magnification using an inverted fluorescence microscope (Ti-E-V5.30, Nikon, Tokyo, Japan) and appropriate filter settings ($\lambda_{\text{ex}} = 549 \text{ nm}$; $\lambda_{\text{em}} = 565 \text{ nm}$ for Actin Red and $\lambda_{\text{ex}} = 330\text{--}380 \text{ nm}$; $\lambda_{\text{em}} = 435\text{--}485 \text{ nm}$ for DAPI). Phase contrast and fluorescence images were analyzed using the open source software ImageJ provided by the NIH [42]. To measure the cell size of individual fibroblasts we analyzed fluorescence images, which were recorded with 40x magnification, with the ImageJ feature 'Analyze particles'. 20 cells per sample were analyzed by manually adjusting the grayscale threshold, and the size distribution was displayed using the software GraphPad Prism (San Diego, CA). The results of the cell area analysis were evaluated using one-way ANOVA and *t*-test analysis for simple linear regression. Statistical analysis was carried out with the software Graphpad Prism, and *p*-values less than or equal to 0.05 were considered statistically significant. Four independent experiments ($n = 4$) with triplicates were conducted. The data of these experiments are presented as mean \pm standard deviation. Statistical parameters including the standard deviation, linearity, and normal distribution were determined. To study the cell morphology with a higher resolution we subsequently performed confocal microscopy using a LSM880 system with Airyscan (Carl Zeiss, Oberkochen, Germany).

2.5. Live cell tracking

DiI perchlorate (1,1-Dioctadecyl-3,3,3,3-tetramethylindocarbocyanine perchlorate, Fisher Scientific) was used to stain the lipid membrane during live cell tracking of 3T3 fibroblasts on different collagen scaffolds. $5 \mu\text{l}$ of 1 mM DiI perchlorate in ethanol was added to $995 \mu\text{l}$ DMEM medium. After fibroblasts were cultivated on the different collagen scaffolds for 24 h, the DiI solution was added and incubated for 30 min at 37°C . Subsequently, live cell tracking was performed with our Nikon inverted fluorescence microscope using a 20x magnification and appropriate filter settings ($\lambda_{\text{ex}} = 549 \text{ nm}$; $\lambda_{\text{em}} = 565 \text{ nm}$). Over 20 h, images were collected with a pco.edge 4.2 LT CMOS camera (PCO, Kelheim, Germany) at 2 min intervals using the Nikon NIS-Elements AR tracking module. Live cell tracking was conducted in four independent experiments ($n = 4$) with triplicates for each substrate type. To ensure statistical relevance, videos with less than 20 tracks were excluded from

the velocity analysis. Tracking data (position data) were imported in the data analysis package IGOR (Wavemetrics, Lake Oswego, OR, USA) for further analysis. Velocities were calculated in a 20 min window (i.e. from 10 or 4 position data depending on the frame rate of the video), where the window is sliding over the entire video sequence by shifting it by 10 min. These velocity data (typically 10 000 to 50 000 data points per sample type) were investigated for differences between the different collagen topographies. Since velocity data showed a log-normal distribution, the logarithm of the velocity was considered here, which showed a normal (Gaussian) distribution (see SI, section S5, available online at <https://stacks.iop.org/BF/13/015007/mmedia>). Since case numbers were very high, even the tiniest differences would show up as statistically significant. Thus, we first calculated a measure for the size of differences by using Cohen's *d*. Cohen's *d* was the difference between two statistical samples (here two different topography types) normalized by the combined standard deviation, i.e. by the geometrical mean of the two standard deviations. Since the velocity histograms showed a main peak at around 50 to 100 nm min⁻¹ and a secondary peak at very low velocities (at around 1 to 10 nm min⁻¹, see figure S-5, which basically corresponds to non-mobile cells and reflects the accuracy of our position data, the mean and standard deviation values used for calculating Cohen's *d* were obtained from a Gaussian fit to the main peak of the histogram (see figure S-6). We considered only Cohen's *d* > 0.2 as a significant or large effect [43]. In these cases, significance values obtained from a Student's *t*-test (on the log *v* data) were always considered as highly significant (i.e. < 10⁻⁶). All velocity data were plotted as peak values of log (*v*) (from the Gaussian fit to the histograms) and subsequently displayed as *v* ± standard deviation using the software Graphpad Prism.

2.6. Scanning electron microscopy

To analyze the scaffold topography with scanning electron microscopy (SEM), collagen samples were cross-linked with 2% GA in PBS for 30 min and subsequently washed with 200 mM NH₄HCO₃ and dried under ambient conditions. Dried collagen samples were sputter-coated with 7 nm of gold in a Bal-Tec SCD 005 sputter system (Leica Microsystems). Fixated cells on collagen scaffolds with different topographies were also analyzed with SEM to study the cell morphology on the nanoscale. Cell samples were fixated using 2% GA solution. To analyze the cell shape after 36 h, additional samples were cultivated and fixated with 2% GA solution. All cell samples were dried with an ethanol exchange series as described earlier [44] before they were coated with gold. SEM analysis of collagen scaffolds and cell samples was carried out in a Zeiss Auriga field emission device (Carl Zeiss,

Oberkochen, Germany) using an operation voltage of 3 kV. Fiber diameters of three individual collagen nanofiber samples per concentration were analyzed using the ImageJ plugin BoneJ [45].

3. Results

3.1. Collagen morphology

When collagen self-assembly was carried out in an ultrasonication bath, we obtained porous networks of collagen nanofibers after drying (see figure 1 and SI, figure S-1). The fiber morphology was preserved upon cross-linking with GA, and ultrasonication yielded a 100% surface coverage of nanofibers on glass substrates. Nanofibers assembled with collagen concentrations of 0.5 mg ml⁻¹ exhibited a distinct fiber morphology with diameters of 136 ± 5 nm (see figure S-1(A)). On the other hand, when higher concentrations of 2.5 mg ml⁻¹ were used, the nanofiber network was less porous with single nanofibers aggregating into larger fiber bundles with individual nanofiber diameters of 149 ± 12 nm (see figure 1(A)). Using cross-sectional SEM analysis of dried nanofibrous scaffolds, we observed a scaffold thickness between 200 and 600 nm for 0.5 mg ml⁻¹ collagen (see figure S-1(B)) and much higher values between 4 and 7 μm for 2.5 mg ml⁻¹ collagen (see figure 1(B)). Similarly, smooth collagen scaffolds prepared with 0.5 mg ml⁻¹ collagen were approximately 400 nm thick (see figure S-1(E)), whereas smooth samples fabricated with 2.5 mg ml⁻¹ collagen ranged from 8 to 10 μm (see figure 1(E)). Hence, by adjusting the collagen concentration we were able to control the scaffold thickness for both, nanofibrous and smooth, collagen scaffolds.

To evaluate the influence of an aqueous cell culture environment on the nanotopography, we rehydrated nanofibrous and smooth collagen in DMEM cell culture medium. AFM analysis of rehydrated scaffolds in deflection mode revealed that the fiber morphology was preserved for both protein concentrations (see figures 1(C) and S-1(C)). Overall, by AFM analysis of the height profiles, we observed that dry and rehydrated nanofibers prepared with 0.5 mg ml⁻¹ collagen exhibited a lower roughness than thick scaffolds fabricated with 2.5 mg ml⁻¹ (see SI, figure S-2 and table S-1). Upon rehydration of collagen nanofibers in DMEM, we found a roughness increase for both collagen concentrations, which was most pronounced for thick scaffolds. Overall, after rehydration the roughness of thin fibrous scaffolds was found to be 1.5-fold higher than for smooth collagen, while a 5-fold increase was observed for thick collagen nanofibers in comparison to the corresponding smooth samples.

To measure the stiffness of nanofibrous and smooth collagen scaffolds after cross-linking, we exemplarily performed AFM measurements (see SI, section S2). Thereby, we observed that both scaffold

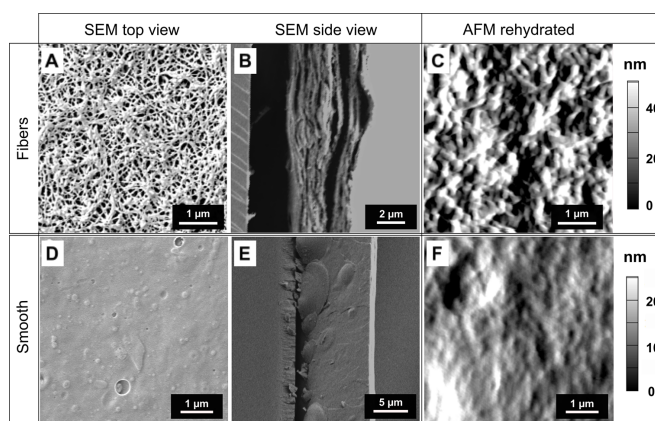


Figure 1. Topography of thick nanofibrous collagen (A to C) in comparison to smooth collagen scaffolds (D to F), both prepared with 2.5 mg ml^{-1} collagen. SEM images of dried scaffolds in top view show topographical differences between collagen nanofibers (A) and smooth collagen (D). SEM images of dried scaffolds in side view display the thickness of nanofibrous collagen (B) and smooth collagen (E). AFM scans show the deflection data of collagen nanofibers (C) and smooth collagen (F), which were both rehydrated in DMEM cell culture medium.

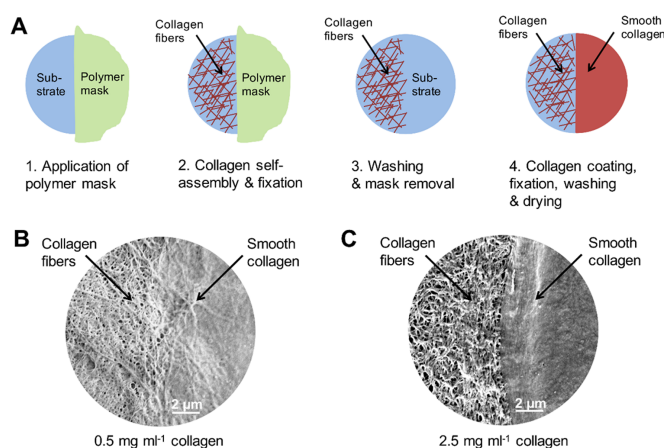


Figure 2. Preparation of binary collagen scaffolds with patterned nanofibrous and smooth topographies. (A) Scheme of the preparation process: 1. The substrate is partly covered with a polymer mask. 2. Collagen nanofibers are assembled on the uncovered substrate area and fixated with 2% GA. 3. Cross-linked collagen fibers are washed with $200 \text{ mM NH}_4\text{HCO}_3$ and the mask is removed. 4. Smooth collagen is coated onto the remaining substrate part, followed by cross-linking with 2% GA, washing with $200 \text{ mM NH}_4\text{HCO}_3$ and a final drying step. SEM images of binary protein scaffolds prepared with (B) 0.5 mg ml^{-1} and (C) 2.5 mg ml^{-1} collagen show a clear border between nanofibrous and smooth topography on the surface.

types were too stiff to be measured with the soft MLCT Bio cantilevers used in this study (data not shown). Independent of the scaffold thickness, the mechanical characteristics of both collagen topographies thus approached the stiffness of bare glass substrates, which is known to exceed 1 GPa [46].

3.2. Binary collagen scaffolds with nanofibrous and smooth topography

To study cell growth in dependence of nanofibrous and smooth collagen topographies, we established a new procedure to prepare protein substrates, which combine regions of nanofibrous and smooth topographies in the same scaffold. As shown in the schematic workflow in figure 2(A), we combined polymer patterning with self-assembly of collagen nanofibers and subsequent coating with smooth collagen. After the initial assembly of nanofibers was

carried out, cross-linking with GA enabled us to prepare a smooth collagen layer on the other substrate half. This procedure could be applied to thin binary scaffolds prepared from 0.5 mg ml^{-1} collagen (see figure 2(B)), as well as to thick scaffolds fabricated with 2.5 mg ml^{-1} collagen (see figure 2(C)). SEM analysis revealed that the differences in nanofibrous and smooth surface topography were more pronounced for thick than for thin collagen patterns.

With this process, we succeeded for the first time in producing collagen matrices with spatially controlled variations in topography within the same scaffold. Using this new scaffold platform, we were now able to conduct comparative studies on the interaction of fibroblasts with nanofibrous and smooth collagen topographies on a single substrate without inducing any variations in the scaffold stiffness or the biochemical composition.

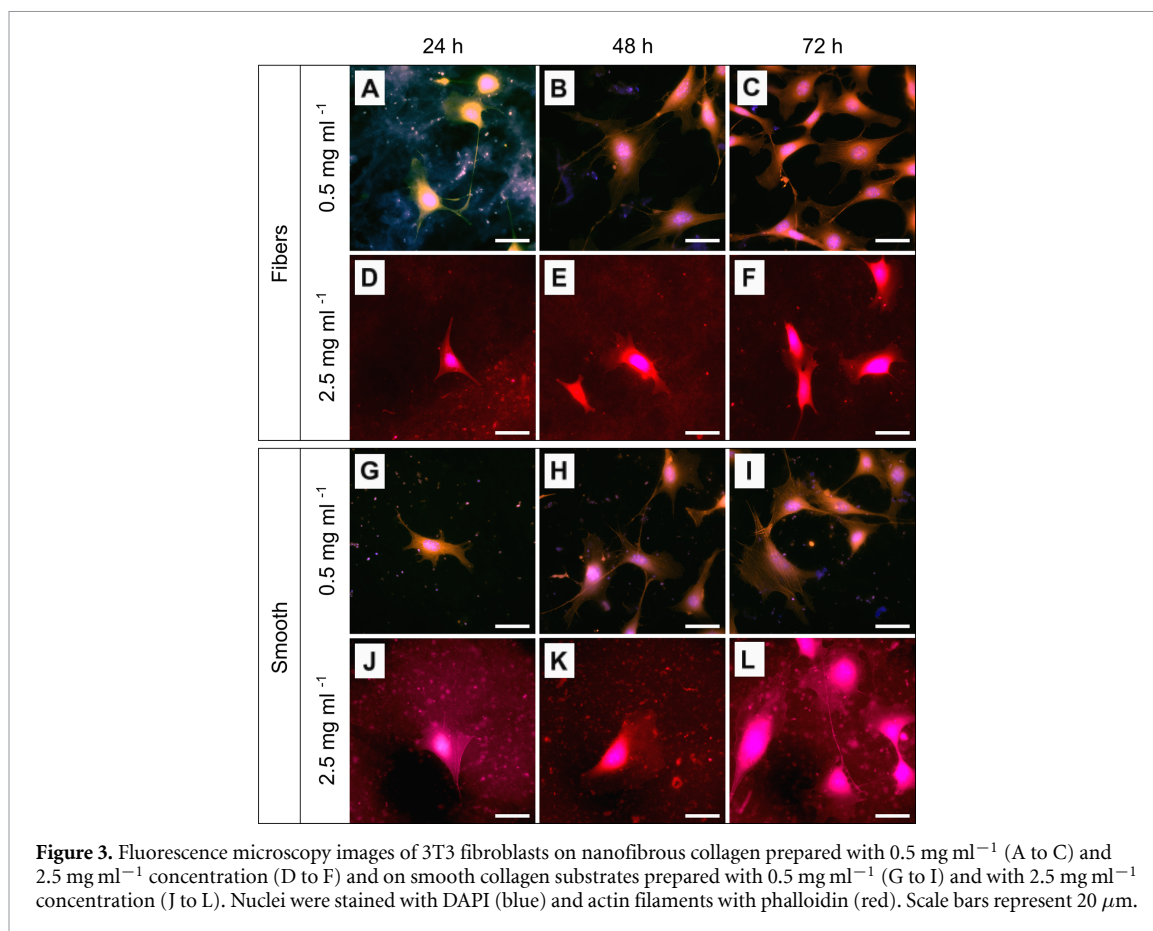


Figure 3. Fluorescence microscopy images of 3T3 fibroblasts on nanofibrous collagen prepared with 0.5 mg ml^{-1} (A to C) and 2.5 mg ml^{-1} concentration (D to F) and on smooth collagen substrates prepared with 0.5 mg ml^{-1} (G to I) and with 2.5 mg ml^{-1} concentration (J to L). Nuclei were stained with DAPI (blue) and actin filaments with phalloidin (red). Scale bars represent $20 \mu\text{m}$.

3.3. Fibroblast interaction with collagen scaffolds

Using a live/dead staining assay (for details see SI section S3), we observed that NIH 3T3 fibroblasts remained viable on nanofibrous and smooth collagen scaffolds, which were prepared with 0.5 mg ml^{-1} protein concentration (see figure S-3). Over 72 h in culture, the fibroblast viability on all samples was between 84% and 98%, indicating a good biocompatibility of both collagen topographies, which was comparable to bare glass substrates. Up to 72 h, we subsequently analyzed the cell morphology with phalloidin staining of the actin cytoskeleton using fluorescence microscopy (see figure 3). Independent of the collagen concentration, 3T3 fibroblasts on collagen nanofibers showed a spindle-like and more elongated morphology with long filopodia (figures 3(A–F)). On the other hand, fibroblasts cultivated on smooth collagen were found to be more flat and larger than cells on collagen nanofibers (figures 3(G–L)). After 48 h in culture, the observed morphological differences were most pronounced. Smooth scaffold regions yielded pronounced actin filaments while actin stress fibers on nanofibrous collagen were substantially reduced.

When we analyzed the size of individual fibroblasts on thin collagen scaffolds, which were prepared with 0.5 mg ml^{-1} collagen, we observed different trends between 24 and 72 h in culture (see figure 4). The largest fibroblasts were found on smooth collagen after 24 h with a cell size of $1796 \pm 581 \mu\text{m}^2$,

differing significantly from those on collagen nanofibers ($p \leq 0.001$) and on glass controls ($p \leq 0.0001$). After 24 h, cells on collagen nanofibers had an average area of $1233 \pm 344 \mu\text{m}^2$; however, cells on glass only exhibited a lower average cell size of $901 \pm 288 \mu\text{m}^2$. Although the overall fibroblast size on nanofibrous and smooth collagen decreased around 48 h and remained at lower values until 72 h in culture, the significant difference in cell size between nanofibers and smooth scaffolds remained unchanged. At this time point, fibroblasts on nanofibrous collagen exhibited a cell area of $959 \pm 214 \mu\text{m}^2$ and cells on smooth collagen showed an area of $1497 \pm 288 \mu\text{m}^2$ ($p \leq 0.01$). At the same time, the cell size of fibroblasts on glass increased to $1151 \pm 309 \mu\text{m}^2$ after 72 h. Overall, the initial differences in fibroblast size between the different substrates were found to be less pronounced after 72 h in culture.

To study the observed differences in fibroblast morphology in dependence of the underlying topography in more detail, we subsequently carried out confocal microscopy and SEM analysis (see figure 5). Since changes in fibroblast morphology were found to be independent of the protein concentration, we used nanofibrous and smooth collagen scaffolds with 4 to $7 \mu\text{m}$ in thickness, prepared with 2.5 mg ml^{-1} collagen, to study whether fibroblast filopodia protruded into the nanofibrous collagen scaffolds. Confocal

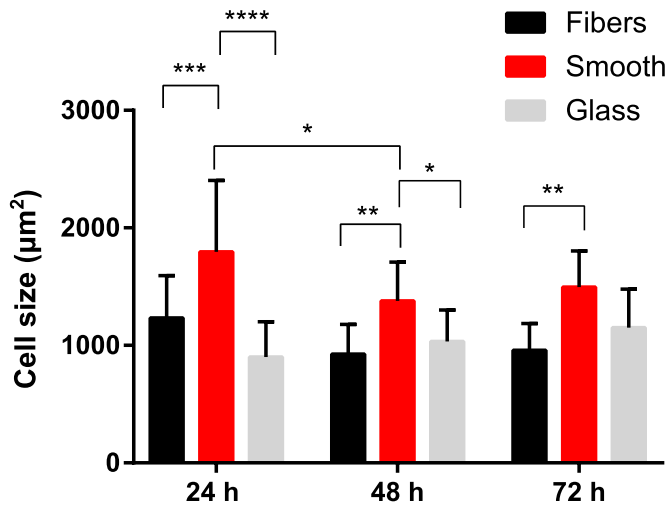


Figure 4. Single cell area of 3T3 fibroblasts cultivated on thin fibrous and smooth collagen prepared with 0.5 mg ml^{-1} collagen and on glass references were evaluated after 24 h, 48 h and 72 h cultivation time. $n = 4$ independent experiments were conducted. Data are presented with average \pm standard deviation of replicates. Significant differences are indicated by * $p \leq 0.05$, ** $p \leq 0.01$, *** $p \leq 0.001$, **** $p \leq 0.0001$.

microscopy and SEM analysis of 3T3 fibroblasts after 24 h, 48 h and 72 h in culture clearly confirmed the differences in morphology and size, which we previously observed with fluorescence microscopy. While 3T3 fibroblasts on collagen nanofibers only exhibited few long cell extensions, fibroblasts on smooth collagen exhibited many short filopodia. Confocal microscopy revealed that 3T3 fibroblast filopodia did not protrude into the nanofibrous collagen scaffolds despite the porous fiber network.

Subsequently, we used AFM to study whether the observed variations in fibroblast morphology were accompanied by changes in cell stiffness (see SI, section S4). AFM measurements of 3T3 fibroblasts revealed a Young's modulus in the range of approximately 1400 to 2500 Pa (see figure S-4) for cells on smooth and nanofibrous collagen scaffolds. Since both collagen scaffolds did not vary in substrate stiffness but only in topography, we could show with these results that fibroblast mechanics were not influenced by the topography of the collagen scaffolds.

3.4. Cell migration on collagen scaffolds

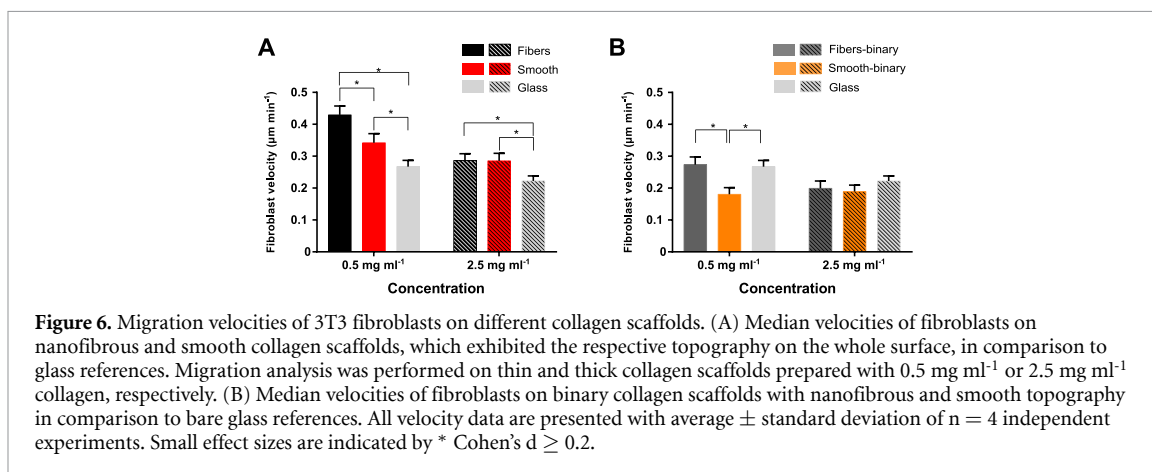
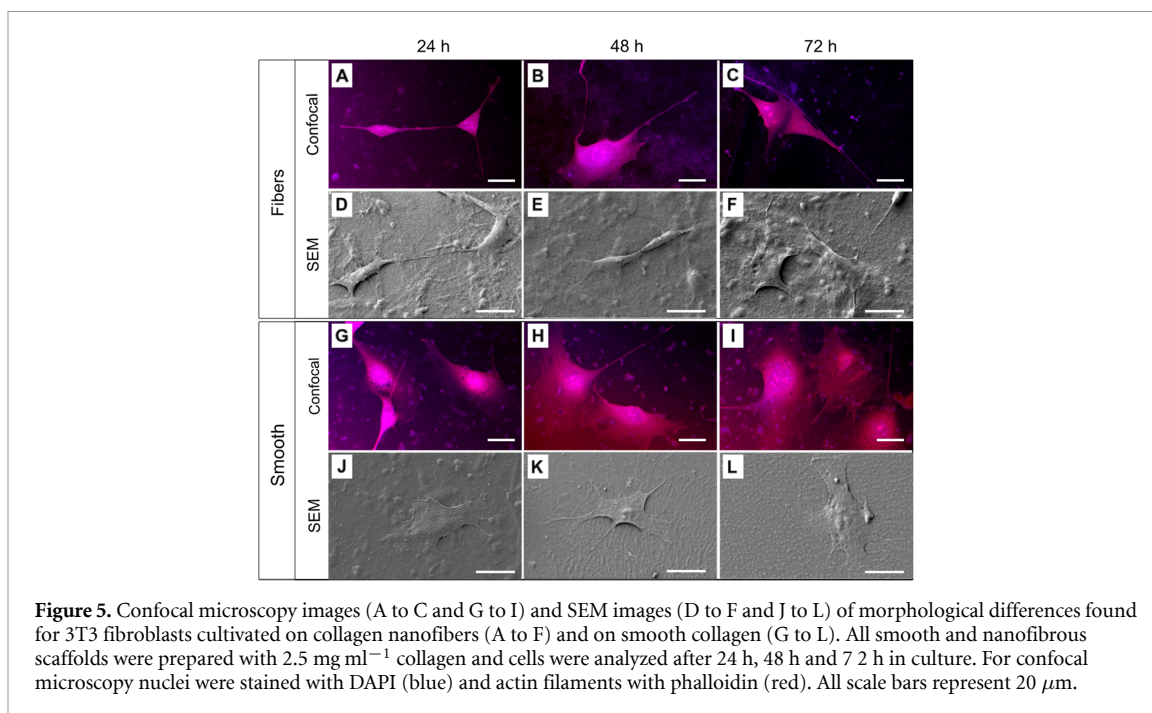
To study how the migration of 3T3 fibroblasts is influenced by the underlying collagen topography, we carried out live cell tracking after cells had initially adhered to the scaffolds for 24 h. Subsequently, over 20 h, the velocity of individual cells was tracked on collagen nanofibers, smooth collagen and binary scaffolds. Thin collagen scaffolds were fabricated with 0.5 mg ml^{-1} collagen while thick scaffolds were prepared with 2.5 mg ml^{-1} collagen. Analysis of cell tracking data was performed as described in the SI section S5 and the results are shown in figure 6.

Figure 6(A) shows the highest migration velocity of more than $0.43 \pm 0.03 \text{ } \mu\text{m min}^{-1}$ for fibroblasts on thin nanofibrous collagen scaffolds (full black bar)

while thin smooth collagen yielded lower velocities around $0.34 \pm 0.03 \text{ } \mu\text{m min}^{-1}$ (full red bar). Hence, on thin collagen nanofibers fibroblasts showed a faster migration than on smooth collagen. With Cohen's $d \geq 0.2$, these topography-dependent differences in fibroblast velocity on thin collagen were found to exhibit a small effect size.

On glass references, fibroblasts exhibited migration velocities between $0.22 \pm 0.02 \text{ } \mu\text{m min}^{-1}$ and $0.27 \pm 0.02 \text{ } \mu\text{m min}^{-1}$ for both concentration series (light grey bar and hatched light grey bar). Independent of the collagen concentration, 3T3 fibroblasts were found to migrate faster on nanofibrous and smooth collagen scaffolds than on glass references. For this trend we found a small effect size of Cohen's $d \geq 0.2$. Interestingly, for thick collagen scaffolds, no topography-dependent velocity differences were observed between nanofibrous and smooth collagen, which both exhibited velocities around $0.29 \pm 0.02 \text{ } \mu\text{m min}^{-1}$ (hatched black and hatched red bars).

On binary collagen patterns (see figure 6(B)), the overall migration velocity of 3T3 fibroblasts was lower than on scaffolds, which exhibited the respective topography over the whole scaffold surface (see figure 6(A)). For binary scaffolds we observed the highest fibroblast velocity of $0.27 \pm 0.02 \text{ } \mu\text{m min}^{-1}$ on thin fibrous collagen regions (dark grey bar), that were in the same range as the respective glass reference (light grey bar). The lowest velocity of $0.18 \pm 0.02 \text{ } \mu\text{m min}^{-1}$ was found for fibroblasts on thin smooth collagen areas (orange bar). With a small effect size of Cohen's $d \geq 0.2$, fibroblasts on nanofibrous areas of thin binary scaffolds migrated faster than on the corresponding smooth regions (dark grey vs. orange bars). This observation agrees well with the trend we previously observed in figure 6(A) for



scaffolds, which exhibited the respective topography over the whole scaffold surface. On thick collagen scaffolds with binary topographies fibroblast velocities of $0.20 \pm 0.02 \mu\text{m min}^{-1}$ were observed for nanofibrous areas while smooth areas yielded velocities of $0.19 \pm 0.02 \mu\text{m min}^{-1}$. Again, this result is consistent with our observations for thick collagen scaffolds, which exhibited the respective topography on the whole surface (see figure 6 (A)).

When fixated fibroblasts on binary collagen scaffolds were analyzed by SEM after 36 h in culture, i.e. in a time window during which live cell tracking was carried out, we could show that the previously observed differences in cell morphology also occurred when fibroblasts migrated from one topographical region to the other (see figure 7). For both scaffold thicknesses, we found fibroblasts, which grew directly on the boundary between nanofibrous and smooth collagen. These cells exhibited short but many

filopodia on the smooth scaffold part, while few and long filopodia protruded from the cell bodies on the nanofibrous scaffold region.

4. Discussion

For the first time, we introduced a new biophysical model system to study cell interaction with nanofibrous and smooth protein topographies in a single scaffold. Using collagen as a model system, we combined *in vitro* self-assembly with polymer printing and tailored cross-linking to fabricate binary protein scaffolds with spatially controlled areas of nanofibrous and smooth topography. With 130 to 150 nm the diameter of dried collagen nanofibers was in good agreement with previous studies on self-assembled collagen [33]. By introducing ultrasonication into this process, we achieved collagen fiber coverages of 100% on the glass surfaces. This is an

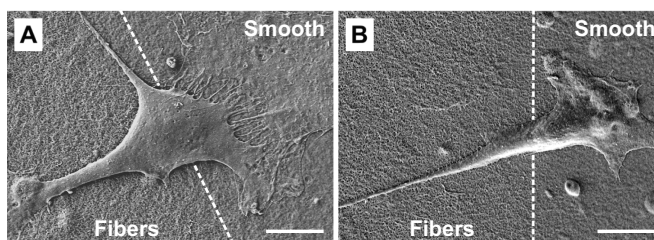


Figure 7. SEM images of fibroblasts on binary collagen scaffolds after 36 h in culture. (A) Thin binary scaffolds were prepared with 0.5 mg ml^{-1} collagen. (B) Thick scaffolds were assembled with 2.5 mg ml^{-1} collagen. For both concentrations, fibroblasts growing on the border between nanofibrous and smooth collagen exhibited many short filopodia on the smooth area while longer filopodia were observed on the nanofibrous scaffold region. Scale bars represent $10 \mu\text{m}$.

improvement in comparison to previously reported fiber coverages of 45%, where collagen self-assembly was carried out in a microfluidic device [47]. By adjusting the protein concentration, we were able to tailor the scaffold thickness between 200 nm and $7 \mu\text{m}$ for collagen nanofibers and between 400 nm and $10 \mu\text{m}$ for smooth collagen. This is in contrast to previous studies, where a pre-patterning with SAMs was required and only collagen patterns up to 47 nm height could be prepared [48]. Moreover, since collagen self-assembly is driven by a pH shift and an increase of ionic strength in the buffer system [31, 32], this process is independent of the underlying substrate material. Therefore, our patterning approach could in future also be applied to other surfaces than glass slides.

To further optimize our binary topography scaffolds for future cell culture studies, it will be important to lower the scaffold stiffness to mimic the mechanical cues of the native ECM more closely [24, 49]. Moreover, the scaffold thickness needs to be increased while maintaining the structure-function relationship to provide a 3D matrix with micron-sized collagen fiber bundles, into which cells can migrate [26, 50]. In our patterning process only the protein topography was tailored, while mechanical and biochemical cues remained unchanged. Therefore, our new scaffold design could become a powerful tool to disentangle topographical from mechanical substrate cues when studying the behavior of different cell types [24]. Towards high precision patterning of protein nanotopographies, it will be advantageous to combine our proof-of-concept process with microcontact printing [51]. Other techniques, like electrospinning or extrusion through nanoporous membranes, would not be suited for such a process combination, since these processes require the successive deposition of fibers on a substrate, often using rotating mandrels [52–54].

In our subsequent cell culture studies with NIH 3T3 fibroblasts, all collagen scaffolds promoted fibroblast adhesion, overall cell viability and migration. Confocal microscopy revealed that 3T3 fibroblast filopodia did not protrude into the porous collagen scaffolds and fibroblasts only adhered to

the surface of the nanofibrous networks. In nature, collagen molecules are covalently cross-linked by members of the lysyl oxidase enzyme family, which also determines the ECM stiffness [15, 55]. Cells are able to migrate through the LOX-cross-linked fiber network of the ECM by proteolytic and non-proteolytic mechanisms [56, 57]. Since we used GA to chemically cross-link collagen scaffolds, we assume that fibroblast filopodia were not able to protrude into the fibrous network using their native migration mechanisms. In order to investigate whether cell filopodia can protrude into porous scaffolds it will therefore be important to adapt the cross-linking procedure in our patterning process, which will simultaneously change the mechanical stiffness [24]. Other cross-linking strategies could, for instance, involve riboflavin-UV treatment, 1-Ethyl-3-(3-dimethylaminopropyl)-carbodiimide or transglutaminase, which are well known to preserve the topography of collagen nanofibers in cell culture studies [58–60].

Variations in collagen topography were found to have the strongest effect on fibroblast morphology and filopodia formation. Smooth scaffold regions yielded cell growth with large contact areas, pronounced actin filaments and many short filopodia. On the other hand, nanofibrous collagen induced spindle-like fibroblast growth with smaller cell sizes, few long cell extensions and substantially reduced actin stress fibers. These morphological differences agree well with previous reports of fibroblast growth on randomly oriented collagen nanofibers [36–38]. Previously, the amount of focal adhesion proteins was found to differ between 2D and 3D scaffolds [23] and the limited available surface area of porous nanotopographies was associated with a reduction in focal adhesion formation [61]. These correlations were confirmed by our observation of reduced actin fiber formation on nanofibrous collagen areas. Since it is not yet understood which mechanisms in filopodia sensing account for their multiple functions [3, 19], it will be highly interesting to further develop our 2D scaffolds with binary topography towards much thicker 3D matrices by tailoring the protein concentration to enable studies of

topography-dependent cell adhesion and migration processes in real time.

In comparison to previous studies on cell mechanics in different microenvironments [49, 62–64], our AFM analysis revealed that fibroblast stiffness was mainly influenced by the scaffold stiffness, regardless of the underlying topography. Analysis of the migration velocity of 3T3 fibroblasts on smooth, nanofibrous and binary collagen scaffolds yielded overall migration velocities between $0.2 \mu\text{m min}^{-1}$ and $0.4 \mu\text{m min}^{-1}$, which corresponds to a velocity range of 12 to $24 \mu\text{m h}^{-1}$. This range is in good agreement with fibroblast migration on other nanostructured substrates, such as cell-derived matrices and collagen gels [36], poly(urethane acrylate) (PUA) nanopatterns [65, 66] or PMMA nanopillars [67]. For fibroblast migration on cell-derived matrices and nanofibrous collagen or fibrin, Hakkinen *et al* reported migration velocities, which were between 1.3 and 1.7 times faster than on the respective 2D scaffolds [36]. On thin collagen scaffolds we observed migration speeds that were between 1.3 and 1.5 times higher on nanofibrous collagen than on smooth collagen, which agrees well with the previous findings reported by Hakkinen *et al*. Nevertheless, for thick collagen scaffolds, we found comparable migration velocities for smooth and nanofibrous collagen, both being reduced in comparison to the migration speed on thin collagen scaffolds. Previously, it was shown that nanotopographies reduce the surface area which is accessible for 3T3 fibroblasts, thereby leading to increased cell migration [61]. Since thick collagen nanofibers exhibited a much higher roughness than thin nanofiber scaffolds, we assume that these differences may have induced the observed variations in migration speed.

Interestingly, fibroblasts on scaffolds with binary topographies showed slower migration velocities than on scaffolds with only one topography. Since binary collagen scaffolds were also prepared on 15 mm glass slides, the respective nanofibrous and smooth areas were reduced by a factor of two, so that a lower total track number was analyzed compared to scaffolds with only one topography. In contrast to substrates with only one topography, nanofibrous regions of binary scaffolds were cross-linked twice (see steps 2 and 4 in figure 2), which made it possible to fabricate scaffolds with two different topographies in the first place. Therefore, more aldehyde residues may have been present on the binary scaffolds, which might have reduced the overall cell migration on substrates with two topographies. However, it was previously observed that increased cross-linking times induce stiffening of collagen hydrogels [68]. Since a variety of cell types is known to respond to stiffer substrates with increased migration rates [69–71], it will be very important in the future to specifically adjust the mechanical cues in different topographical scaffold regions.

Towards a versatile biophysical model system, it will be highly interesting to apply our patterned self-assembly process to other fibrillar proteins, which form nanofibrous scaffolds upon self-assembly. A very promising candidate is the blood plasma protein fibrinogen, for which we recently introduced the new process of salt-induced self-assembly to prepare 3D nanofiber scaffolds [72, 73]. At the same time, fibrinogen could be processed into smooth scaffolds, and cross-linking in formaldehyde was found to preserve both topographies in aqueous environment [73]. By transferring our patterning approach to other fibrillar proteins, it might also become possible to selectively modify biochemical and mechanical cues in different scaffold regions. Such a multiparametric scaffold platform with tailored topography, substrate stiffness and biochemical cues in defined scaffold areas could enable us to gain fundamental insight into cellular recognition processes during adhesion and migration. With regard to future applications in tissue engineering, it would also be advantageous to combine different fibrillar proteins in the same patterned scaffold to address different cell types of a tissue, for instance via integrin-specific adhesion, in combination with different topographic cues. Such scaffold designs could also pave the way for new co-culture systems to optimally steer the growth of different cell types in regenerative medicine.

5. Conclusion

Using collagen as a model protein, we have introduced a new process of patterned self-assembly to produce protein scaffolds with spatially controlled variations of smooth and nanofibrous topography. In this new scaffold platform, the surface topography was varied without changing the biochemical or mechanical scaffold characteristics. Using our binary collagen scaffolds, we observed topography-induced changes in fibroblast morphology from small, spindle-shaped cells with reduced actin cytoskeleton on nanofibers to large, flat fibroblasts with many short filopodia and dense actin filaments on smooth collagen regions. In the future, our new scaffold platform could open up exciting possibilities for tracking the time dependence of topography-induced recognition processes in individual cells. This unique setup could allow us to distinguish between local and systemic reactions of cells to topographical cues. Moreover, it could become possible to transfer the results of conventional smooth 2D cell culture systems directly to the development of nanofibrous 3D scaffolds. Furthermore, our study could form the basis for a multiparametric scaffold platform, in which topographical, mechanical and chemical cues can be independently varied to investigate their respective influence on cell growth.

Acknowledgments

The authors thank Professor Walter Lang from the Institute for microsensors, -actuators and -systems (IMSAS) at the University of Bremen for access to the scanning electron microscope. Annette Peter is gratefully acknowledged for her support in confocal microscopy. We also thank Eva Eilers for her support in cell culture experiments. The authors gratefully acknowledge funding by the Emmy Noether program of the German Research Council under Grant No. BR 5043/1-1.

ORCID iD

Dorothea Brüggemann  <https://orcid.org/0000-0002-7140-3275>

References

- [1] Ventre M and Netti P A 2016 Engineering cell instructive materials to control cell fate and functions through material cues and surface patterning *ACS Appl. Mater. Interfaces* **8** 14896–908
- [2] Nguyen A T, Sathé S R and Yim E K F 2016 From nano to micro: topographical scale and its impact on cell adhesion, morphology and contact guidance *J. Phys. Condens. Matter.* **28** 183001
- [3] Gupton S L and Gertler F B 2007 Filopodia: the fingers that do the walking *Sci. STKE* **2007** 1-8
- [4] Albuschies J and Vogel V 2013 The role of filopodia in the recognition of nanotopographies *Sci. Rep.* **3** 1–9
- [5] Bettinger C J, Langer R and Borenstein J T 2009 Engineering substrate topography at the Micro- and nanoscale to control cell function *Angew. Chem., Int. Ed.* **48** 5406–15
- [6] Biggs M J P, Richards R G and Dalby M J 2010 Nanotopographical modification: A regulator of cellular function through focal adhesions *Nanomed. Nanotechnol. Biol. Med* **6** 619-33
- [7] Dalby M J, Gadegaard N and Oreffo R O C 2014 Harnessing nanotopography and integrin-matrix interactions to influence stem cell fate *Nat. Mater.* **13** 558–69
- [8] Kim D H, Provenzano P P, Smith C L and Levchenko A 2012 Matrix nanotopography as a regulator of cell function *J. Cell Biol.* **197** 351–60
- [9] Carlson A L *et al* 2016 Generation and transplantation of reprogrammed human neurons in the brain using 3D microtopographic scaffolds *Nat. Commun.* **7** 1-10
- [10] Sridharan R, Cameron A R, Kelly D J, Kearney C J and O'Brien F J 2015 Biomaterial based modulation of macrophage polarization: a review and suggested design principles *Mater. Today* **18** 313-25
- [11] Tawfick S, De Volder M, Copic D, Park S J, Oliver C R, Polsen E S, Roberts M J and Hart A J 2012 Engineering of micro- and nanostructured surfaces with anisotropic geometries and properties *Adv. Mater.* **24** 1628-74
- [12] Ermis M, Antmen E and Hasirci V 2018 Micro and Nanofabrication methods to control cell-substrate interactions and cell behavior: a review from the tissue engineering perspective *Bioact. Mater.* **3** 355–69
- [13] Sales A, Ende K, Diemer J, Kyvik A R, Veciana J, Ratera I, Kemkemer R, Spatz J P and Guasch J 2019 Cell type-dependent integrin distribution in adhesion and migration responses on protein-coated microgrooved substrates *ACS Omega* **4** 1791–800
- [14] Petreaca M and Martins-Green M 2013 *The Dynamics of Cell-ECM Interactions, with Implications for Tissue Engineering* (Amsterdam: Elsevier)
- [15] Frantz C, Stewart K M and Weaver V M 2010 The extracellular matrix at a glance *J. Cell Sci.* **123** 4195-200
- [16] Halper J and Kjaer M 2014 Basic components of connective tissues and extracellular matrix: elastin, fibrillin, fibulins, fibrinogen, fibronectin, laminin, tenascins and thrombospondins *Adv. Exp. Med. Biol.* **802** 31-47
- [17] Ploetz C, Zycband E I and Birk D E 1991 Collagen fibril assembly and deposition in the developing dermis: segmental deposition in extracellular compartments *J. Struct. Biol.* **106** 73-81
- [18] Fang M, Goldstein E L, Matich E K, Orr B G and Banaszak Holl M M 2013 Type I collagen self-assembly: the roles of substrate and concentration *Langmuir* **29** 2330–8
- [19] Jacquemet G, Hamidi H and Ivaska J 2015 Filopodia in cell adhesion, 3D migration and cancer cell invasion *Curr. Opin. Cell Biol.* **36** 23–31
- [20] Fraley S I, Feng Y, Krishnamurthy R, Kim D H, Celedon A, Longmore G D and Wirtz D 2010 A distinctive role for focal adhesion proteins in three-dimensional cell motility *Nat. Cell Biol.* **12** 598–604
- [21] Duval K, Grover H, Han L H, Mou Y, Pegoraro A F, Fredberg J and Chen Z 2017 Modeling physiological events in 2D vs. 3D cell culture *Physiology* **32** 266–77
- [22] Cukierman E, Pankov R and Yamada K M 2002 Cell interactions with three-dimensional matrices *Curr. Opin. Cell Biol.* **14** 633-9
- [23] Cukierman E, Pankov R, Stevens D R and Yamada K M 2001 Taking cell-matrix adhesions to the third dimension *Science* **294** 1708–12
- [24] Yang Y, Wang K, Gu X and Leong K W 2017 Biophysical regulation of cell behavior—cross talk between substrate stiffness and nanotopography *Engineering* **3** 36-54
- [25] Grinnell F and Petroll W M 2010 Cell motility and mechanics in three-dimensional collagen matrices *Annu. Rev. Cell Dev. Biol.* **26** 335–61
- [26] Walters B D and Stegemann J P 2014 Strategies for directing the structure and function of three-dimensional collagen biomaterials across length scales *Acta Biomater.* **10** 1488–501
- [27] Kim H S, Lee D Y, Park J H, Kim J H, Hwang J H and Jung H I 2007 Optimization of electrohydrodynamic writing technique to print collagen *Exp. Tech.* **31** 15–19
- [28] Kwak E A, Ahn S and Jaworski J 2015 Microfabrication of custom collagen structures capable of guiding cell morphology and alignment *Biomacromolecules* **16** 1761–70
- [29] Desai R A, Khan M K, Gopal S B and Chen C S 2011 Subcellular spatial segregation of integrin subtypes by patterned multicomponent surfaces *Integr. Biol.* **3** 560–7
- [30] Monroe M R, Li Y, Ajinkya S B, Gower L B and Douglas E P 2009 Directed collagen patterning on gold-coated silicon substrates via micro-contact printing *Mater. Sci. Eng. C* **29** 2365–9
- [31] Elsdale T and Bard J 1972 Collagen substrata for studies on cell behavior *J. Cell Biol.* **54** 626–37
- [32] Kadler K E, Holmes D F, Trotter J A and Chapman J A 1996 Collagen fibril formation *Biochem. J.* **316** 1–11
- [33] Li Y, Asadi A, Monroe M R and Douglas E P 2009 pH effects on collagen fibrillogenesis *in vitro*: electrostatic interactions and phosphate binding *Mater. Sci. Eng. C* **29** 1643–9
- [34] Parenteau-Bareil R, Gauvin R and Berthod F 2010 Collagen-based biomaterials for tissue engineering applications *Materials* **3** 1863–87
- [35] Plant A L, Bhadriraju K, Spurlin T A and Elliott J T 2009 Cell response to matrix mechanics: focus on collagen *Biochim. Biophys. Acta, Mol. Cell Res.* **1793** 893–902
- [36] Hakkinen K M, Harunaga J S, Doyle A D and Yamada K M 2011 Direct comparisons of the morphology, migration, cell adhesions, and actin cytoskeleton of fibroblasts in four different three-dimensional extracellular matrices *Tissue Eng. Part A* **17** 713–24

- [37] Jiang H and Grinnell F 2005 Cell-matrix entanglement and mechanical anchorage of fibroblasts in three-dimensional collagen matrices *Mol. Biol. Cell* **16** 5070–6
- [38] Stylianou A, Yova D and Alexandratou E 2013 Nanotopography of collagen thin films in correlation with fibroblast response *J. Nanophotonics* **7** 073590
- [39] Huang N F, Lai E S, Ribeiro A J S, Pan S, Pruitt B L, Fuller G G and Cooke J P 2013 Spatial patterning of endothelium modulates cell morphology, adhesiveness and transcriptional signature *Biomaterials* **34** 2928–37
- [40] Francis-Sedlak M E, Uriel S, Larson J C, Greisler H P, Venerus D C and Brey E M 2009 Characterization of type I collagen gels modified by glycation *Biomaterials* **30** 1851–6
- [41] Lee K, Choi S, Yang C, Wu H C and Yu J 2013 Autofluorescence generation and elimination: A lesson from glutaraldehyde *Chem. Commun.* **49** 3028–30
- [42] Rueden C T, Schindelin J, Hiner M C, DeZonia B E, Walter A E, Arena E T and Eliceiri K W 2017 ImageJ2: ImageJ for the next generation of scientific image data *BMC Bioinform.* **18** 1–26
- [43] Cohen J 2013 *Statistical Power Analysis for the Behavioral Sciences* (New York: Academic Press)
- [44] Brüggemann D 2010 *Nanostrukturierte Metallelektroden zur funktionalen Kopplung an neuronale Zellen* Vol. 9 (Jülich: Forschungszentrum Jülich GmbH)
- [45] Doube M, Klosowski M M, Arganda-Carreras I, Cordelières F P, Dougherty R P, Jackson J S, Schmid B, Hutchinson J R and Shefelbine S J 2010 BoneJ: free and extensible bone image analysis in ImageJ *Bone* **47** 1076–9
- [46] Inaba S, Fujino S and Morinaga K 2004 Young's modulus and compositional parameters of oxide glasses *J. Am. Ceram. Soc.* **82** 3501–7
- [47] Spurlin T A, Forry S P, Cooksey G A and Plant A L 2010 Characterization of collagen fibrils films formed on polydimethylsiloxane surfaces for microfluidic applications *Langmuir* **26** 14111–7
- [48] Elliott J T, Woodward J T, Umarji A, Mei Y and Tona A 2007 The effect of surface chemistry on the formation of thin films of native fibrillar collagen *Biomaterials* **28** 576–85
- [49] Discher D E, Janmey P and Wang Y L 2005 Tissue cells feel and respond to the stiffness of their substrate *Science* **310** 1139–43
- [50] Baker B M and Chen C S 2012 Deconstructing the third dimension-how 3D culture microenvironments alter cellular cues *J. Cell Sci.* **125** 3015–24
- [51] Alom Ruiz S and Chen C S 2007 Microcontact printing: A tool to pattern *Soft Matter* **3** 168–77
- [52] Matthews J A, Wnek G E, Simpson D G and Bowlin G L 2002 Electrospinning of collagen nanofibers *Biomacromolecules* **3** 232–8
- [53] Raoufi M, Aslankoohi N, Mollenhauer C, Boehm H, Spatz J P and Brüggemann D 2016 Template-assisted extrusion of biopolymer nanofibers under physiological conditions *Integr. Biol.* **8** 1059–66
- [54] Sell S A, Boland E D, Simpson D G and Bowlin G L 2007 Nanofiber technology: designing the next generation of tissue engineering scaffolds *Adv. Drug Deliv. Rev.* **59** 1413–33
- [55] Walker C, Mojares E and Del Río Hernández A 2018 Role of extracellular matrix in development and cancer progression *Int. J. Mol. Sci.* **19** 1–31
- [56] Wolf K and Friedl P 2011 Extracellular matrix determinants of proteolytic and non-proteolytic cell migration *Trends Cell Biol.* **21** 736–44
- [57] Bonnans C, Chou J and Werb Z 2014 Remodelling the extracellular matrix in development and disease *Nat. Rev. Mol. Cell Biol.* **15** 786–801
- [58] Spurlin T A, Bhadriraju K, Chung K H, Tona A and Plant A L 2009 The treatment of collagen fibrils by tissue transglutaminase to promote vascular smooth muscle cell contractile signaling *Biomaterials* **30** 5486–96
- [59] Gruschwitz R, Friedrichs J, Valtink M, Franz C M, Müller D J, Funk R H W and Engelmann K 2010 Alignment and cell-matrix interactions of human corneal endothelial cells on nanostructured collagen type I matrices *Investigative Ophthalmol. Vis. Sci.* **51** 6303–10
- [60] Lai E S, Anderson C M and Fuller G G 2011 Designing a tubular matrix of oriented collagen fibrils for tissue engineering *Acta Biomater.* **7** 2448–56
- [61] Frey M T, Tsai I Y, Russell T P, Hanks S K and Wang Y L 2006 Cellular responses to substrate topography: role of myosin II and focal adhesion kinase *Biophys. J.* **90** 3774–82
- [62] Haase K and Pelling A E 2015 Investigating cell mechanics with atomic force microscopy *J. R. Soc. Interface* **12** 1–16
- [63] Rianna C and Radmacher M 2017 Influence of microenvironment topography and stiffness on the mechanics and motility of normal and cancer renal cells *Nanoscale* **9** 11222–30
- [64] Viji Babu P K, Rianna C, Belge G, Mirastschijski U and Radmacher M 2018 Mechanical and migratory properties of normal, scar, and Dupuytren's fibroblasts *J. Mol. Recognit.* **31** 1–11
- [65] Kim D H, Han K, Gupta K, Kwon K W, Suh K Y and Levchenko A 2009 Mechanosensitivity of fibroblast cell shape and movement to anisotropic substratum topography gradients *Biomaterials* **30** 5433–44
- [66] Kim J *et al* 2017 Directional matrix nanotopography with varied sizes for engineering wound healing *Adv. Healthcare Mater.* **6** 1700297
- [67] Liang E I, Mah E J, Yee A F and Digman M A 2017 Correlation of focal adhesion assembly and disassembly with cell migration on nanotopography *Integr. Biol.* **9** 145–55
- [68] Pilipchuk S P, Vaicik M K, Larson J C, Gazyakan E, Cheng M H and Brey E M 2013 Influence of crosslinking on the stiffness and degradation of dermis-derived hydrogels *J. Biomed. Mater. Res. A* **101** 2883–95
- [69] Pathak A and Kumar S 2012 Independent regulation of tumor cell migration by matrix stiffness and confinement *Proc. Natl Acad. Sci. USA* **109** 10334–9
- [70] Lange J R and Fabry B 2013 Cell and tissue mechanics in cell migration *Exp. Cell Res.* **319** 2418–23
- [71] Kai F B, Laklai H and Weaver V M 2016 Force matters: biomechanical regulation of cell invasion and migration in disease *Trends Cell Biol.* **26** 486–97
- [72] Stapelfeldt K, Stamboroski S, Mednikova P and Brüggemann D 2019 Fabrication of 3D-nanofibrous fibrinogen scaffolds using salt-induced self assembly *Biofabrication* **11** 025010
- [73] Stapelfeldt K, Stamboroski S, Walter I, Suter N, Kowalik T, Michaelis M and Brüggemann D 2019 Controlling the multiscale structure of nanofibrous fibrinogen scaffolds for wound healing *Nano Lett.* **19** 6554–63